Fundamentals of High Temperature Processes

Behaviour of cavity formation and convection in $FeOx–SiO_2$ melts under plasma arc

K.MATSUMARU et al.

The behaviour of oxides melted by plasma arc has been studied. Oxides of FeOx and $FeOx–SiO_2$ were melted by argon plasma arc. A direct-current-transferred type plasma generator was employed. Observations of the sample surface revealed that a cavity formed in the region where the plasma arc was directed and that surface flow was operative in the direction from the centre toward the edge of the melt. The depth of the cavity was governed by the balance between the hydrostatic pressure and the sum of the pressures caused by the arc and the argon gas flow. The main driving force of convection on the sample surface was the aerodynamic drag force. The temperature distribution was dependent on both the argon gas flow rate and the viscosity of the sample, because the heat from the plasma arc was mostly transported by convection on the sample surface.

Sulphide capacities of "FeO"–SiO_2, CaO–"FeO", and "FeO"–MnO slags

M.M.NZOTTA et al.

In view of the lack of sulphide capacity data for iron oxide-bearing slags that are of great importance in metallurgical processes, the present work was initiated to study the sulphide capacities of "FeO"–SiO_2, "FeO"–CaO, and "FeO"–MnO melts. The melts were equilibrated with a gas mixture of CO, CO_2, SO_2 and Ar with known sulphur and oxygen partial pressures in the temperature range of 1 623 to 1 873 K. The quenched slag samples were analysed for sulphur contents by the stoichiometric combustion method. Chemical analyses were also carried out to determine the chemical composition of the slag in view of the dissolution of iron and manganese from the slag into the platinum containers. The experimental results were compared with those obtained by other investigators and the thermodynamic aspects are discussed. On the basis of a sulphide capacity model developed in the present laboratory, the sulphide capacities in these three binary systems have been described as functions of temperature and composition.

Thermodynamic fundamentals for alumina-content control of oxide inclusions in Mn–Si deoxidation of molten steel

S.KOBAYASHI

In the deoxidation producing the $MnO–SiO_2–Al_2O_3$ inclusions, the significant ununiformity in the temperature dependence of equilibrium constant among the deoxidation reactions may cause the inclusions to change in their composition in cooling processes till solidification of steel melt. The present work concerns the compositional variation of the inclusions formed in the Mn–Si deoxidation of steel, focused on alumina content in the cooling process from 1 848 to 1 773 K.

In order to take the mass balances of the components involved in a reaction system, a reaction region was introduced which consisted of liquid steel bath and a certain amount of the oxides belonging to added flux and refractory of refining vessels. The compositional variation of the inclusions was estimated on the basis of the deoxidation equilibria and the mass balances. The thermodynamic analysis has revealed that the composition of inclusions has such a temperature dependence as to be considerably influenced by the initial total contents of reactants involved in the deoxidation system. It is suggested that high total contents of aluminum and oxygen in the initial state reduce the temperature dependence and thereby will facilitate the composition control in the cooling process till solidification.

In Mn–Si deoxidation, there may be two approaches to control alumina content of inclusions; one is to leave the target composition once attained at an appropriate temperature till solidification intact, and the other is to form inclusions stable on temperature falling through regulating the initial total contents of aluminum and oxygen to adequately high levels.

Wettability effects on bubble characteristics in a bubbling wall jet along a vertical flat plate

N.SONOYAMA et al.

Experimental investigation was carried out to reveal the effect of the wettability of a vertical flat plate on a bubbling jet rising along the plate. Two flat plates with different contact angles of $\theta=62°$ and 104° were used, being classified into a good and a poor wettability plate, respectively. Bubble frequency, gas holdup, mean bubble rising velocity and mean bubble chord length were measured with a two-needle electroresistivity probe. When the wettability of a plate was poor, bubbles were likely to rise in the close vicinity of the plate and some of them attached to the plate. As a result, the mean bubble rising velocity and mean bubble chord length thus measured in the close vicinity of the plate were dependent significantly on the wettability of the plate. The horizontal distributions of the bubble frequency were similar in an axial region where the buoyancy force acting on bubbles governs the flow field. The same was true for the horizontal distributions of the gas holdup.

Dispersion of primary inclusions of Ce_2O_3 and CeS in Fe–0.20mass%C–0.02mass%P alloy

M.GUO et al.

In order to introduce primary inclusions uniformly into a liquid steel, the experiments on the coalescence and separation by flotation of the deoxidation product of Ce_2O_3 or CeS particles were carried out at 1 873 K in an Fe–0.20mass%C–0.02mass%P alloy. It was found that the size and number of particles were strongly dependent on the holding time at 1 873 K and the cooling rate. The number and size of clusters and those of particles in a cluster in a polished cross-section were metallographically examined. The spatial particle size distribution, which was obtained by applying the Schwartz–Saltykov transformation to the observed planar size distribution, was studied as a function of holding time at 1 873 K. From the plot in the probability graph, the log-normal distribution was found to be a good approximation for the spatial particle size. The contents of insoluble Ce obtained from chemical analysis were compared with those estimated from the data for particle size distribution by using various methods.

Viscosities of some fayalitic slags containing CaF_2

F.SHAHBAZIAN et al.

In an effort to systematize the knowledge of the viscosities of slags containing CaF_2 and to enable the prediction of the change of viscosities of mould flux slags, viscosity measurements of synthetic slags in the system "FeO"–SiO_2–CaF_2 were carried out in the temperature range 1 450–1 763 K. Five different fayalite slag compositions with "FeO" contents varying between 55–65 mass% in the homogeneous liquid range were chosen for the studies. The CaF_2 content was varied between 5 and 15 mass%. Due to the reactions between the slag components and CaF_2, some CaO was formed during the premelting of the slags. Through analysis, it was found that, compositional changes due to fluoride evaporation occurred during the long premelting period. The libration of the volatile components SiF_4 and FeF_2 during sample preparation was the main source for compositional changes. DTA experiments were carried out in order to determine the liquidus points of the slags studied. CaF_2 was found to decrease the liquidus temperatures.

The viscosities were measured by the rotating cylinder method using spindles and crucibles made of iron in an argon atmosphere. The results showed the effect of the CaF_2 content on viscosity. The activation energy for viscous flow was generally dependent on the "FeO"/SiO_2 ratio and viscosity increased with decreasing temperature. The effect on the viscosities of "FeO"–SiO_2 slags due to CaF_2 additions was not found to be as significant as in the case of $CaO–SiO_2$ slags.

Ironmaking

Coal and coke for blast furnaces

H.BERTLING

The main charge material for the steel production is liquid hot metal. It is mainly produced in blast furnaces. The blast furnace operates according to the counter-current principle. The process makes the blast furnace reliant on lumpy materials to maintain a gas-permeable stock column. The most important reducing agent is therefore the lumpy coke. Auxiliary reducing agents, such as coal or oil, are injected via the tuyeres. The tasks of coke and coal for the hot metal production and the requirements of the blast furnace on coal- and coke-quality are described.

The consumption of coal and coke in the blast furnace is met on the one hand by the market or on the other hand by the own production. It depends on the conditions of the market and the availability of production facilities. World-wide the production of hot metal and crude steel via the blast furnace/converter route is regarded as the dominant process line also in future. Consequently, after their successes in

the past, the ironmaking and steelmaking industry have joined their efforts with the cokemaking industry to exploit still more development potentials for hot metal production.

Injection of flux into the blast furnace via tuyeres for optimising slag formation

J.MA

Based on discussion of the slag formation problems occurred during a commercial scale blast furnace test of 100% high Fe-content self-fluxed pellets, a proposal of replacing the charge of flux from the top by injection via tuyeres has been presented. It will optimise the slag formation process and provide a great potential of further increase productivity with smooth operation due to: 1) decrease bosh slag volume significantly; 2) obtain even and proper basicities of primary slag, bosh slag, tuyere slag and final slag formed along the height the blast furnace.

Operation and design of scrap melting process of packed bed type

T.YAMAMOTO et al.

A coke Packed bed type Scrap Melting process (PSM) with simultaneous high-rate injection of oxygen and pulverized coal was proposed which aims to achieve high heat efficiency, high productivity, high Fe yield and low refractory erosion with using not only shaft type furnaces but also basic oxygen converter (BOF) vessel.

The experiments were made to verify the usefulness of the proposed process using the modified experimental blast furnace of 1 ton pig per tap scale and the modified experimental BOF of 10 ton pig per tap scale. A 3-dimensional mathematical simulation model was also developed in order to elucidate the physical and chemical conditions inside the furnace on the basis of transport phenomena and to make a basic design of commercial scale plant. Obtained results were summarized as follows:

1) 100% steel scrap can be melted into well carburized and well desulpherized pig iron using both 1 ton scale blast furnace and 10 ton scale BOF.
2) The heat efficiency of about 80%, the productivity per unit furnace volume of about 50 t/d · m^3, Fe yield of more than 99% and the erosion rate of refractory of less than 0.5 mm/charge were achieved throughout the experiments.
3) These results were well justified by the 3-dimensional mathematical simulation model.
4) A basic design of commercial scale plant was also performed by the use of the model.

Steelmaking

Application of barium-bearing alloys in steelmaking

K.MUKAI et al.

Based on the understanding of the physico-chemical properties of alkaline earth metals, an overview on the investigation of application of Ba-bearing alloys in steel is given in the paper. As calcium it is, barium has a strong affinity for oxygen and sulfur in steel; barium can also modify the inclusions in the steel. The barium-bearing inclusions easily float out from steel. The residual barium-bearing inclusions exist in spherical complex aluminates and randomly distribute in the steel. The mechanical properties such as fatigue, transverse impact toughness and anisotropic properties of steels treated with barium-bearing alloys are improved. The effect of calcium and barium on microstructure of steel is discussed.

Some characteristics of production of barium-bearing alloys are also discussed.

Numerical prediction and experimental verification of thermal stratification during holding in pilot plant production ladles

C. E.GRIP et al.

A 3-dimensional CFD-model has been developed to simulate the natural convection flow in ladles. Qualified measurements of temperature and velocities in 107 and 7 tonne ladles have been made to verify the model. The downward convection flow at the ladle wall has been studied using radioactive isotopes and the thermal stratification has been studied by means of continuous temperature measurements. The experimental techniques are complex and additional numerical simulations have been carried out to study the effect of the measurement technique on the measurement error. The result indicates that the measurements are of sufficient accuracy for the validation. The measurements are compared to predictions from the numerical model. The main conclusion is that the theoretical CFD model gives a very accurate estimation of the temperature distribution during holding.

Casting and Solidification

Influence of dissolved cerium and primary inclusion particles of Ce_2O_3 and CeS on solidification behavior of Fe–0.20mass%C–0.02mass%P alloy

M.GUO et al.

The influence of dissolved Ce and primary inclusion particles of Ce_2O_3 (the planar mean particle diameter, $\bar{d}_A$=1.6 to 2.1 μm) or CeS ($\bar{d}_A$=2.4 to 2.8 μm) on solidification micro- and macrostructure was investigated in an Fe–0.20mass%C–0.02mass%P alloy. The primary and secondary dendrite arm spacings decreased with an increase in the content of dissolved Ce in the range between 140 and 750 mass ppm, but they tended to decrease with increasing the number of Ce_2O_3 or CeS particles up to N_A= 900 mm^{-2}. With an increase in the number of Ce_2O_3 or CeS particles up to N_A=900 mm^{-2}, the area fraction of equiaxed crystals increased from 30 to 55%, but it was found to be independent of the dissolved Ce content. The degree of undercooling reduced by increasing the particle number of Ce_2O_3 or the dissolved Ce content. The correlation between primary dendrite arm spacing and austenite grain size was discussed.

Numerical simulation of peritectic reaction using a multi-phase-field model

J.S.LEE et al.

A multi-phase-field model is applied to simulate the peritectic reaction of Fe–C alloys. The phase-field equations, the diffusion equation for the multi-phase-field model and a dilute solution approximation for the descriptions of the free energy densities are presented. The thin-interface limit of the phase-field model for alloy solidification is employed to obtain the parameters relationship. The calculated results of the peritectic reactions show that the growth rates of the γ phase follow the parabolic growth kinetics in 1-D isothermal transformations and the linear growth kinetics in the 1-D continuous cooling case. During the 2-D peritectic reaction, where liquid, δ and γ phase are in mutual contact, the moving directions of interface are in accord with the driving force of the phase transformation at the interfaces.

Welding and Joining

Welding characteristics of stainless steel in 10 kW laser beam welder

M.ITO et al.

10 kW laser beam welder was installed in the continuous annealing and pickling line for hot coil (H-APL), and welding characteristics was researched. As a result, the following conclusions are obtained. The maximum penetration depth was obtained at the focal point of 2 mm below the surface. The HAZ width of a laser weld was approximately 0.3 mm, and the number of bending repetition and the HAZ width were mutually related.

The deterioration in ZnSe lens was caused by adhesion of fumes, spatters and dusts of welding to the lens surface, or residual strain of lens occurred as the number of welding passes increased. The thermal effect occurred by using deteriorated lens. For prevention of the thermal effect, the parabolic mirror could be used instead of ZnSe lens, since the penetration depths of parabolic mirror and the ZnSe lens were almost equal.

Transformations and Microstructures

Sn segregation and its influence on electrical steel texture development

M.GODEC et al.

During the recrystallization microalloyed Sn in non-oriented electrical steel segregates to the surface and on grain boundary and affects the texture development. In spite of the fact that the grain boundary segregation is much smaller compared to surface segregation, both have an influence on recrystallization and on texture development in electrical steel. Auger electron spectroscopy (AES) was used to measure the grain boundary and surface segregation of Sn in non-oriented electrical steels alloyed with different Sn weight contents (0.025, 0.05 and 0.1%). The grain boundary segregation of the specimens, which were previously aged at 530°C for various times and were fractured under UHV conditions, was measured. The surface segregation temperature dependence and its kinetics were followed in polycrystalline specimens in the temperature range from 400 to 900°C on the grains of known crystallographic orientations: (100), (111) and

(110). The textures were measured by X-ray texture goniometer and the results were presented as orientation distribution functions (ODF). By controlled surface and grain boundary segregation it is possible to achieve the selective grain growth which improves the electrical properties of non-oriented electrical steel. The best results were obtained by alloying it with 0.05 wt% Sn.

Mechanical Properties

Ultrahigh carbon steels, Damascus Steels and ancient blacksmiths

O.D.SHERBY

The processing and mechanical properties of ultrahigh carbon steels (UHCS) have been studied over the past twenty-five years, initially at Stanford University and later at Lawrence Livermore National Laboratory. These studies have shown that such steels (1 to 2.1%C) can be made superplastic at elevated temperature, and have high strength and good ductility at room temperature. The metallurgy of UHCSs is now well understood allowing economical procedures to achieve ultra-fine hypereutectoid spheroidite, pearlite and optically-unresolvable martensite. The investigation of these UHCSs brought us, eventually, to study the history and metallurgy of Damascus steel and Japanese swords, and of ancient blacksmiths. These ancient Persian and Japanese weapons, the most famous in the world, were also ultrahigh carbon steels. It is proposed that the iron age may have begun at the same time period as the early bronze age, approximately 7 000 BC. The Damascus steel age began at about 2 000 BC, the same as the full bronze age.

お詫び

①「鉄と鋼」Vol. 85 (1999) No. 5（平成11年5月号）pp. 405~410に掲載されました論文の和文題目に誤りがございましたので，次のとおり訂正させていただきます。

誤　SUS304L鋼とZr鋼との固相接合継手の耐食性

正　SUS304L鋼とZrとの固相接合継手の耐食性

著者ならびに読者各位にご迷惑をおかけいたしました。お詫びして訂正いたします。

②「鉄と鋼」Vol. 85 (1999) No. 6（平成11年6月号）pp. 454に掲載されました図および写真に一部不鮮明な箇所がございましたので，下記に改めて掲載させていただきます。著者ならびに読者各位にご迷惑をおかけいたしましたことをお詫びいたします。

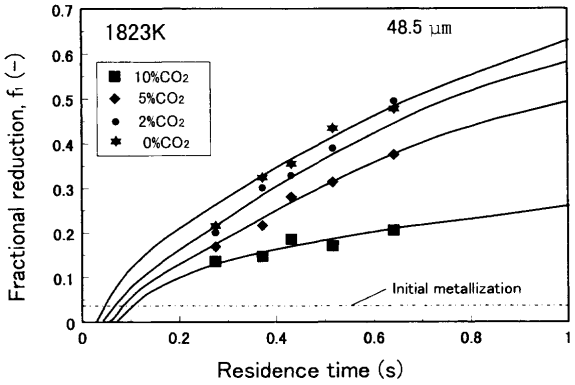

Fig. 3. Relation between fractional reduction and particle residence time at 1823K. (Each curve shows measured results.)

pp. 454　Fig. 3

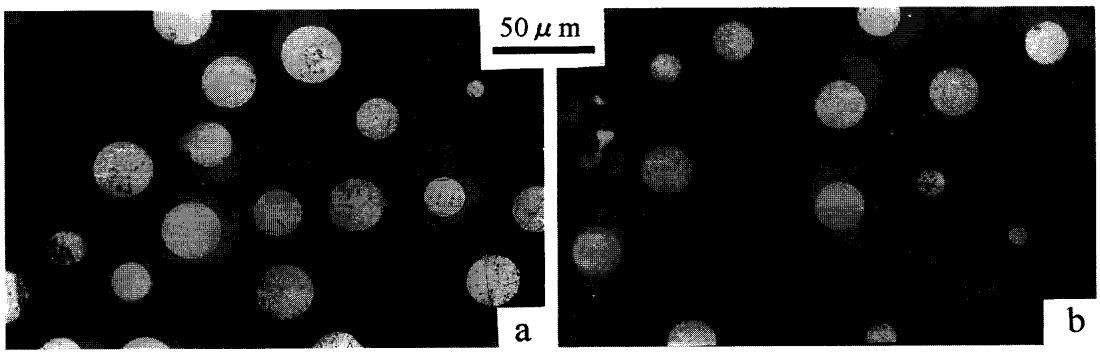

Fig. 4. Cross sections of particles after reduction with 100% CO gas at 1773K, a) Q=0.60 Nl/min, f_1=0.359, τ=0.520 sec, b) Q=1.5 Nl/min, f_1=0.183, τ=0.279 sec.

pp. 454　Fig. 4